Research Article

Sorption Properties of Remazol Navy RGB 150 from an Aqueous Solution onto Activated Carbon Prepared from Posidonia Oceanica Seagrass

Hacer Şensöz[1*], Ramazan Donat[2]

[1] Pamukkale University, Kale Vocational School, https://orcid.org/0000-0002-2173-8974
[2] Pamukkale University, Faculty of Sciences, https://orcid.org/0000-0002-5701-5030
[*]Correspondence: E-mail: hsensoz@pau.edu.tr,
[*]Correspondence: rdonat@pau.edu.tr

(First received February 23, 2024 and in final form May 22, 2024)

Reference: Şenöz, H., Donat, R. Sorption Properties of Remazol Navy RGB 150 from an Aqueous Solution onto Activated Carbon Prepared from Posidonia Oceanica Seagrass. The European Journal of Research and Development, 4(2), 149-167.

Abstract

In this study, adsorption parameters were examined to remove RN- RGB 150 ions from aqueous solutions by using activated carbon obtained from Posidonia Oceanica, which is known as seagrass. The structure of activated carbon derived from Posidonia Oceanica seagrass *was characterized by FTIR, SEM, and BET analysis methods. The significance of parameters such as temperature, solution concentration, adsorbent dosage, and the influence of time on the adsorption performance of RN-RGB 150 ions has been comprehensively investigated. The adsorption of RN-RGB 150 ions onto PO-AC demonstrated exceptional agreement with the Langmuir isotherm model, achieving a remarkable maximum adsorption capacity of 60.97 mg.g^{-1} and an adsorbate density of 0.1519 L m.g^{-1}. This significant finding highlights the potential of PO-AC as a highly effective adsorbent for RN-RGB 150 ions, suggesting its suitability for applications such as wastewater treatment.*

Keywords: *Remazol Navy RGB 150, Sorption, Posidonia Oceanica, Activated Carbon, Dye Adsorption, Wastewater treatment*

1. Introduction

The rapid global population growth and dynamic industrialization processes not only result in the emergence of increasing waste materials but also bring about various ecological and social problems. The increase in industrialization, while carrying the potential to improve living standards, tends to adversely affect the natural habitat of living beings to the same degree. Moreover, the high accumulation of pollutants in the air, water, and soil-in solid, liquid, and gaseous phases from various sources - lays the groundwork for the emergence of environmental problems, including water pollution. Dyes used in the production process in various industrial sectors such as cosmetics, leather, textiles, pharmaceuticals, food, paper, printing, and plastics are among the main pollutants that significantly increase water pollution (Dutta et al., 2021; Nachiyar et al., 2023).

Industries prefer synthetic dyes in contrast with natural ones because they are more cost-effective, offer a wide range of colors, and are easier to use. More than 100 000 commercial dyes and 7×10^5 tons of dyestuffs are produced annually (Pathania et al., 2017; Zhang et al., 2019).

The traditional biological wastewater treatment process can't provide sufficient efficiency for effectively treating wastewater containing dyes due to the low biodegradability of these dyes. In water treatment processes, physical and chemical treatment methods are commonly applied to remove various pollutants and improve water quality (Nachiyar et al., 2023).

Approximately 12% of synthetic dyes are lost during production and processing, and significantly, around 20% of this dye loss contaminates industrial wastewater. This situation indicates that synthetic dyes cause significant environmental problems (Wu et al., 2020).

The release of organic and inorganic pollutants into the environment does cause significant changes in the atmosphere. As a result, pollutants released into the environment can cause significant changes; including water contamination, the death of trees and grasslands, wildlife problems, contamination in the food chain, health issues in flora and fauna, and serious human health problems (Al-Tohamy et al., 2022).

Textile dyes have a detrimental impact on the health of water bodies beyond aesthetics. They increase both biochemical and chemical oxygen demand, hindering photosynthesis and plant growth. Additionally, these dyes enter the food chain and resist degradation (recalcitrance), accumulating in organisms. This raises concerns about potential toxicity,

mutagenicity, and carcinogenicity (Al-Tohamy et al., 2022; Nachiyar et al., 2023). Studies show that many synthetic dyes can be dangerous and even carcinogenic. It has been determined that these dyes can cause serious health problems in humans, including increased heart rate, vomiting, shock, cyanosis, jaundice, quadriplegia, and tissue necrosis (Wanyonyi et al., 2013).

Several approaches exist for tackling the challenge of dye removal in colored industrial discharges. These methods can be divided into three main categories: (i) physical methods such as adsorption (Brião et al., 2018; Madan et al., 2019), membrane filtration (Homem et al., 2019), and flocculation (Liu et al., 2018a); (ii) chemical methods such as chemical oxidation (Aravind et al., 2018; Kang et al., 2019), electrochemical degradation (Wawrzkiewicz et al., 2019; Pereira et al., 2020), and ozonation (Peng et al., 2017; Hien et al., 2020); and (iii) biological degradation methods such as enzyme and microorganism utilization (Nurhadi et al., 2019).

To tackle the challenge of dye wastewater, adsorption has emerged as a popular treatment method. (Kadhom et al., 2020). Adsorption is not only effective for removing organic dyes from wastewater, but it is also cost-effective, simple, and feasible to implement. Many synthetic adsorbents have been used to effectively remove water-soluble contaminants (Rasheed et al., 2020; Bożęcka et al., 2021). The selection of an adsorbent material significantly impacts its efficiency and effectiveness. Key factors to consider include the functional groups present on its surface, the overall pore structure, and the presence of micropores and mesopores, which all contribute to the material's adsorption capacity (Bulgariu et al., 2019; Hassan et al., 2020).

Activated carbon is one of the most effective and widely used adsorbents in the treatment of dye wastewater, thanks to its large specific surface areas, large pore volumes, chemical inertness, and robust mechanical stability (Li et al., 2016). However, the production of activated carbon may not be cost-effective due to the high temperature and lengthy duration required (Yang and Qiu 2010). Due to the high cost of producing activated carbon, researchers are exploring alternative, lower-cost materials like algal residues (Chang et al., 2015; Reda and Sayed, 2018), seaweed (Gokulan et al., 2019; Kumar et al., 2021), orange peel (Stella Mary et al., 2016; Obaid and Ali 2023), clays (Dawood et al., 2018), tea waste (Goswami and Phukan 2017; Liu et al., 2018b), rice husk (Ding et al., 2014; Zhang et al., 2015), olive seeds (Albadarin and Mangwandi, 2015) and, fishbone (Belessi et al., 2009).

Alg-based processes are generally options that can be easily implemented compared to other traditional treatment methods, and they are often the most operational, economical, and environmentally friendly choices (Pandya et al., 2017; Samei et al., 2019).

2. Materials and Methods

The reactive textile dyestuff Remazol Navy RGB 150 (RN-RGB 150) (obtained commercially) was investigated as a potential adsorbent in this study. Samples of PO-AC accumulated on the shores of the Aegean Sea (Figure 1.a) were collected and washed in the laboratory with plenty of water to remove salinity. Following the experiment, the samples underwent drying in a temperature-controlled oven at 100°C±5°C. A 600-gram portion of the dried *Posidonia Oceanica* seagrass sample was placed in the reactor and subjected to a carbonization process at a high temperature of 600°C. After tar and wood vinegar were heated at 600°C, physical activation was achieved by sending water vapor into the containers for thirty minutes. As a result of the process, 140.10 grams of activated carbon from *Posidonia Oceanica* seagrass (PO-AC) were obtained with a mass loss of 76.65%. The produced adsorbent material was mechanically ground and sieved to obtain powder with different particle sizes. The resulting particle size fractions were: <20, (20-63), >63, <70, and >125µm.

(a) (b)

Figure 1: (a) Posidonia Oceanica (b) Activated Carbon Obtained from Posidonia Oceanica

2.1. Application of Adsorption Experiment

For use in adsorption experiments, a stock solution was prepared by dissolving 0.926 g of RN-RGB 150 dye substance in 1 liter of distilled water. To achieve the desired working solution concentrations (115.8, 231.5, 463, and 694.5 $mg.L^{-1}$), these solutions were diluted. To achieve homogeneity, 10 mL of representative samples of the solutions were weighed and added to the predetermined amount of biosorbent. The mixture was then thoroughly mixed. Adsorption studies were conducted under batch conditions using appropriate

amounts of adsorbate and adsorbent in 25 mL of erlenmeyer flaks, and during this process, a ZHWY-200B model incubator shaker was utilized for shaking. Samples in a temperature-controlled shaking incubator were analyzed at specific times after being withdrawn periodically. Each solution's pH was adjusted using a WTW brand microprocessor-controlled pH meter. Samples were centrifuged at 5000 rpm for 10 minutes in a Hettich Universal 16A centrifuge. Quantification of the residual RN-RGB 150 concentration in the solution post-adsorption was achieved using a PerkinElmer Lambda 25 model UV-vis spectrophotometer. The concentration of RN-RGB 150 ions was determined spectrophotometrically at a wavelength of 615 nm.

2.2. Characterization

Activated carbon's properties were investigated using the Brunauer-Emmett-Teller (BET) method to determine its surface area, pore volume, pore size distribution, and surface morphology. An investigation of the activated carbon sample's surface morphology and elemental composition was conducted using Scanning Electron Microscopy (SEM). Fourier Transform Infrared Spectroscopy (FTIR) analysis was employed to identify and characterize the functional groups present on the surface of the adsorbent.

2.3. Calculation

The adsorption percentage (%E) and distribution coefficients (K_d) of RN-RGB 150 ions were determined using the relevant equations.

$$\% E = \frac{C_i - C_e}{C_i} x100 \quad (1)$$

$$K_d = \frac{C_i - C_e}{C_e} \frac{V}{m} \quad (2)$$

In the above equations, the notations represent the following parameters: C_i (mg.L^{-1}) Initial concentration of RN-RGB 150 ions before adsorption, C_e (mg.L^{-1}), Equilibrium concentration of RN-RGB 150 ions in the solution after adsorption, V (mL) Volume of the liquid phase, m (g) Mass of the adsorbent. These experiments were carried out by varying parameters such as ambient temperature, dye concentration, and adsorbent dosage to determine their effects on the adsorption efficiency. In the adsorption studies, Langmuir and Freundlich isotherm models were utilized.

2.3.1. Pseudo-first-order model

The first model is based on the assumption that the adsorption of RN-RGB 150 on PO-AC is a reversible process and follows a first order kinetic reaction. The pseudo-first-

order kinetic model proposed by Lagergren is generally expressed by the following equation (Ho, 2014).

$$\frac{dq_t}{dt} = k(q_e - q_t) \quad (3)$$

Where:

q_t = number of RN-RGB 150 ions adsorbed by the PO-AC adsorbent at time t (mg.g^{-1}) q_e = number of RN-RGB 150 ions adsorbed by the PO-AC adsorbent at equilibrium (mg.g^{-1}) k_1 = pseudo-first-order rate constant (min^{-1}).

After integration with boundary conditions ($t = 0$, $q_t = 0$, and $t = t$, $q_t = q_t$) Eq. (3) becomes,

$$\log(q_e - q_t) = \log\ q_e - \frac{k_1}{2.303} t \quad (4)$$

by plotting $\log(q_e - q_t)$ against t. The t_1 and q_e values can be calculated from the slope and intercept of a straight line on a graph (Gupta et al., 2012).

2.3.2. Pseudo second order model

This model was presented by Ho (2014) and is expressed by the equation:

$$\frac{dq_t}{d_t} = k(q_e - q_t)^2 \quad (5)$$

After integration with boundary conditions ($t = 0$, $q_t = 0$, and $t = t$, $q_t = q_t$) then Equation (5) becomes,

$$1/q_t = \frac{1}{k_2(q_e)^2} + \frac{1}{q_e} \quad (6)$$

Where k_2 is a pseudo-second-order rate constant (g.min^{-1}mg^{-1}). The k_2 and q_e values can be calculated from the intercept and slope of the linear line on the graph if you plot (t/q_t) vs. t.

The Langmuir sorption isotherm is a model used to describe equilibrium sorption processes. It assumes that the adsorbent surface has a finite number of identical adsorption sites. Sorption occurs as a monolayer, meaning only one layer of adsorbate molecules can occupy the surface.

The Langmuir equation is expressed by the following formula (Langmuir, 1916):

$$\frac{C_e}{q_e} = \frac{1}{Q_{max} b_L} + \frac{C_e}{Q_{max}} \quad (7)$$

The symbols used in the Langmuir equation are as follows: C_e represents the equilibrium concentration of RN-RGB 150 ions in the solution; q_e represents the amount of RN-RGB 150 ions adsorbed on the adsorbent; Q_{max} represents the monolayer adsorption capacity; and b_L represents the energy parameter.

The Freundlich model is a mathematical model used to describe the multilayer adsorption process of physico-chemical interactions between adsorbate molecules and heterogeneous surfaces. The equation represents the linearized version of the Freundlich isotherm model (Freundlich, 1907).

$$\log q_e = \log K_F + \frac{1}{n_F} log\ C_e \quad (8)$$

In the Freundlich equation, the symbols correspond to the following parameters: q_e is the amount of adsorbate adsorbed per mass of adsorbent at equilibrium; K_F and n_F are Freundlich constants, which express adsorption capacity and density, respectively.

The relations used in calculating the thermodynamic parameters are given in equations (9) and (10) (Saleem et al., 1992; Khan et al., 1995; Akyıl et al., 1998).

$$ln\ K_d = \frac{\Delta S^o}{R} - \frac{\Delta H^o}{RT} \quad (9)$$

$$\Delta G = \Delta H - T\Delta S \quad (10)$$

In the above equations, K_d represents the distribution coefficient, ΔH^o signifies enthalpy, ΔS^o represents entropy, K denotes absolute temperature, and R signifies the gas constant. In the other equation, ΔG represents Gibbs free energy.

3. Results

3.1. Characterization of the Adsorbent

3.1.1. BET Analysis

Nitrogen gas adsorption measurements of the activated carbon sample at 77.42 K were carried out on the Quantachrome Autosorb 1-C device. The BET and Langmuir test results show that activated carbon has a specific surface area of 309.86 and 411.48 $m^2.g^{-1}$, a specific pore volume of 0.206 $cm^3.g^{-1}$, a total pore volume at a relative pressure of 0.984, and an average pore diameter of 26.1 Å.

3.1.2. SEM Analysis

Prior to and following biosorption, the surface morphology of RN-RGB 150 ions was examined using SEM. As depicted in Figure 2, SEM images reveal the surface characteristics of the samples. As shown in Figure 2, the surface of PO-AC was found to have an irregular, rough, and porous structure before adsorption. Adsorption of RN-RGB 150 ions resulted in penetration of the porous structure, leading to increased surface roughness and disruption of the particle morphology.

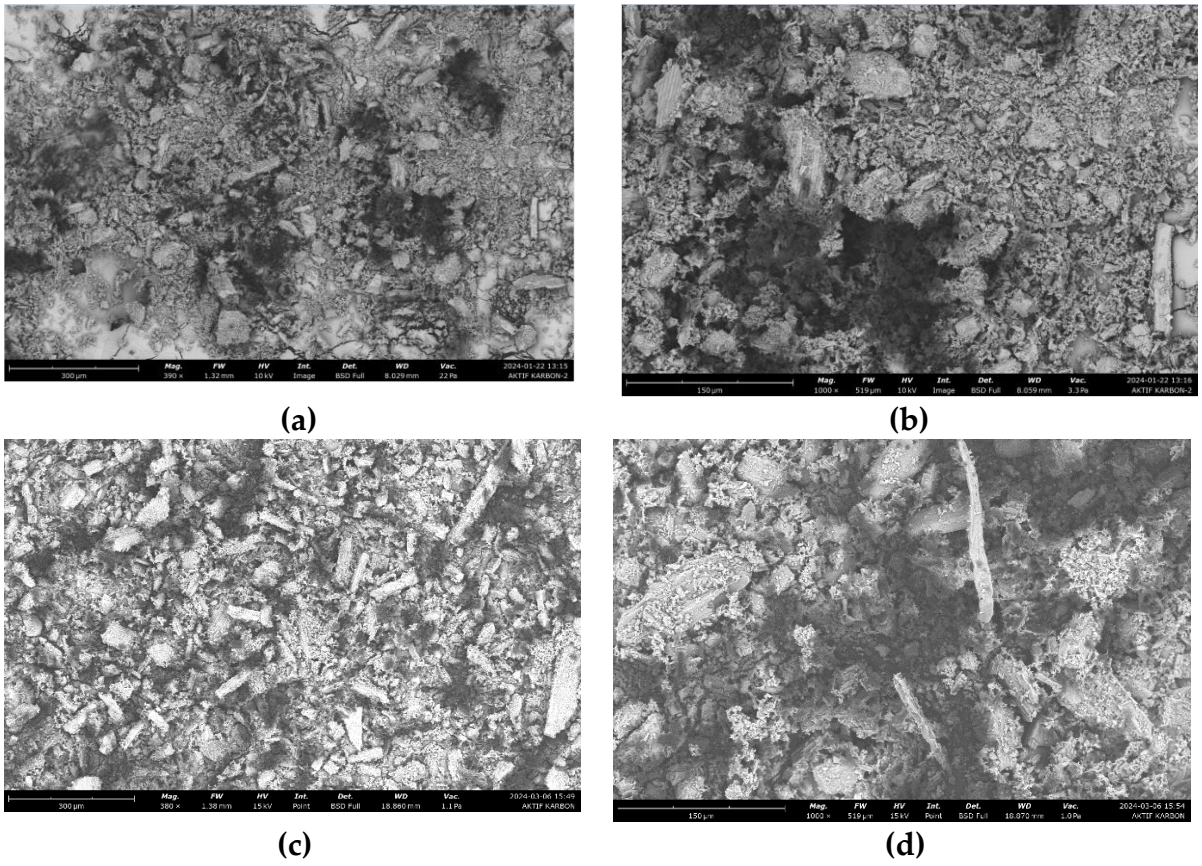

Figure 2: SEM Images of the PO-AC Before (a,b) and After (c,d) Adsorption

3.1.3. FTIR analysis

The FTIR study of functional groups and compounds in samples is crucial for characterizing activated carbon and predicting adsorption effectiveness. The precursor, activating agent, method, and activation circumstances all affect the surface characteristics and functional groups of activated carbon.

The functional groups present in the activated carbon adsorbent both before and after the adsorption of RN-RGB 150 ions were subsequently as certained by analyzing the characterization data. Figure 3. presents the activated carbon adsorbent's FTIR spectrum before and after the adsorption of RN-RGB 150 ions, demonstrating notable variations. There is a wave number shift in the vibration group in the activated carbon adsorbent spectrum following adsorption as compared to the spectrum before adsorption.

The results of the characterization indicate that the functional groups R-COO-, C=C, C=O, C-H, C-N, C-O, and C-C are present in the spectra of PO-AC and RN-RGB 150-loaded PO-AC.

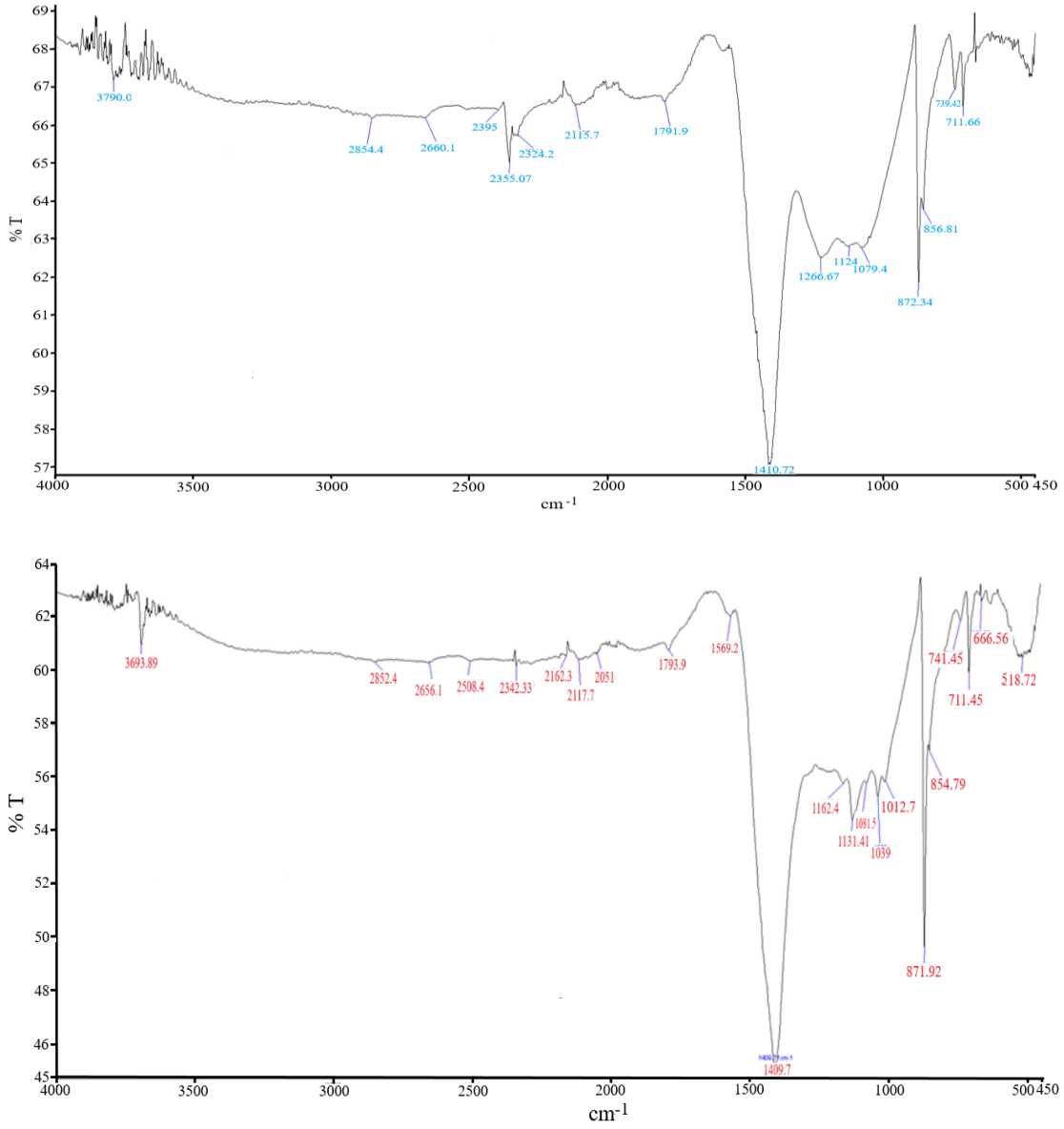

Figure 3: FTIR Spectra of PO-AC Before (a) and After (b) RN-RGB 150 Adsorption

3.2. Adsorption Studies

3.2.1. Effect of Time

The adsorption of a 463 mg.L^{-1} concentration of RN-RGB 150 by PO-AC was investigated using a fixed volume of 25 mL erlenmeyer flask, 0.075 g of adsorbent, a shaking speed of 125 rpm, and a temperature of 303.15 K. The effect of contact time on the study was investigated by conducting experiments at different durations: 15, 30, 60, 90, 120, 180, 240, 360, 480, and 720 minutes (Figure 4). At the end of the 720-minute shake, the adsorption percentage (%E) of RN-RGB 150 ions was determined to be 96.30%, and the equilibrium constant K_d was determined to be 3472.59 mL.g^{-1}. The analysis of the dye removal process revealed a rapid increase in the initial stages of contact time, followed by a decrease in the rate of increase in subsequent stages as contact time increased. Following 300 minutes of shaking, both the adsorption percentage and equilibrium constant approached steady-state values.

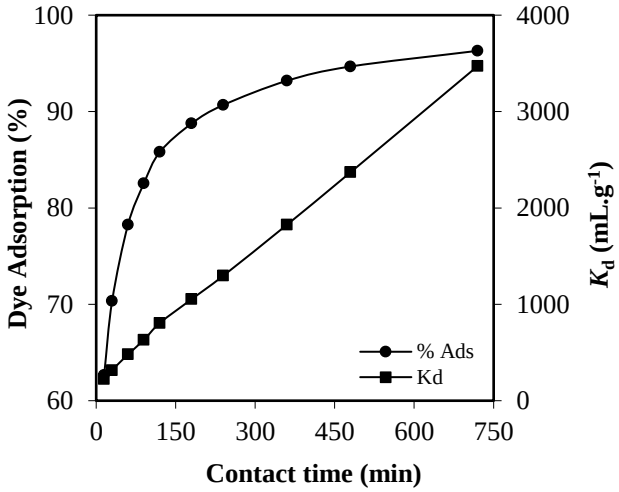

Figure 4: Influence of Contact Time on the Efficiency of RN-RGB 150 Ion Adsorption onto PO-AC (Adsorbent dose = 0.075 g, RN-RGB 150 = 463 mg.L^{-1}, Initial pH = 6.00, Particle size = 20>63 <74µm, Temperature = 303.15 K).

3.2.2. Adsorption Kinetics

The study of adsorption kinetics reveals how quickly an adsorbate accumulates on the surface of an adsorbent, with time playing a crucial role in the process. A shorter contact time to reach adsorption equilibrium signifies a faster adsorption rate. Adsorption rate testing was achieved through reaction order estimation in this study. The rate of a chemical reaction or chemical process is defined as the speed at which a reaction occurs. In this research, adsorption kinetics data were obtained empirically using pseudo-first-

order and pseudo-second-order models. First-order pseudo-equations use equation (4) and second-order equations use equation (6).

The results obtained are as shown in Figure 5 for first-order and Figure 6 for second-order. From the results of theoretical calculations, the pseudo-second-order correlation coefficient (R^2) value is closer to number one (1.00) compared to pseudo-first-order. The first- order pseudo equation has a value of R^2 = 0.491, and the second-order pseudo equation has a value of R^2 = 0.996. This shows that pseudo-second-order modeling makes the adsorption data more representative. If this modeling is in accordance with the experiment, then the adsorption mechanism involves a chemical reaction (chemisorption) between the adsorbate and the adsorbent.

The adsorption rate constant value (k_2) obtained from the intercept value in Figure 6 is 9.61×10^{-6} ($g.mg^{-1}.min^{-1}$), and the amount of adsorbate adsorbed (q_e) is theoretically 322.58 mg adsorbate/g adsorbent.

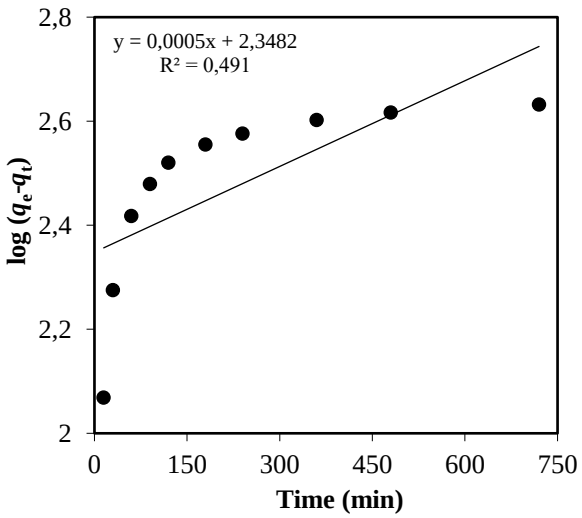

Figure 5: First-Order Kinetic Model

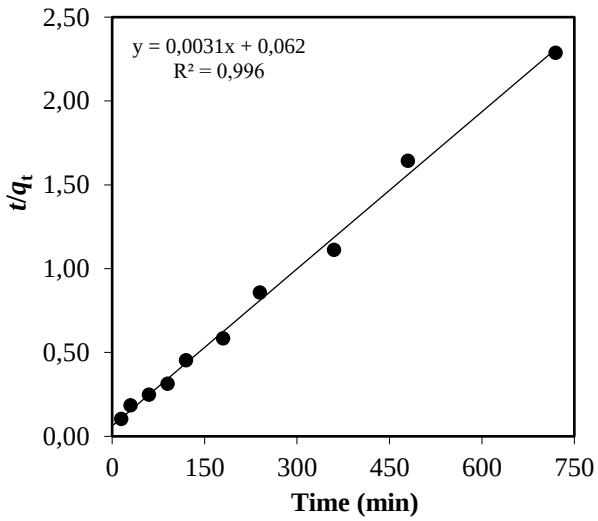

Figure 6: Second-Order Kinetic Model

3.2.3. Effect of Dye Concentration

While adsorption capacity represents the amount of biosorbate retained by the biosorbent, removal percentage is associated with the rate at which the biosorbate transfers from the solution to the biosorbent surface. The effect of adsorbent dosage on the adsorption capacity of PO-AC was investigated in a solution of RN-RGB 150 with an initial concentration of 463 $mg.L^{-1}$. Varying amounts of PO-AC were used: 0.05, 0.075, 0.100, 0.150, 0.175, 0.200, and 0.225 g (Figure 7). The adsorption of RN-RGB 150 by PO-

AC was examined with a fixed volume of 25 erlenmeyer flask for 180 minutes a shake speed of 125 rpm, and a temperature of 303.15 K. As the initial dye concentration decreases, the ratio of dye molecules to active surface area is expected to decline, consequently leading to a greater number of dye molecules binding to the surface (Arabi and Sohrabi, 2014).

As observed in the present study, increasing the dosage of the adsorbent (resulting in a larger mass quantity) provides a greater number of active sites for adsorption. This corroborates the findings reported in the literature, which indicate a positive correlation between dosage and removal percentage (Wanyonyi et al., 2013; Tural et al., 2017). Despite an increase in adsorbent dosage, the constant level of dye adsorption can be attributed to the high dosage promoting the formation of adsorbent aggregates, which subsequently reduce the available surface area for adsorption (Ali et al., 2020).

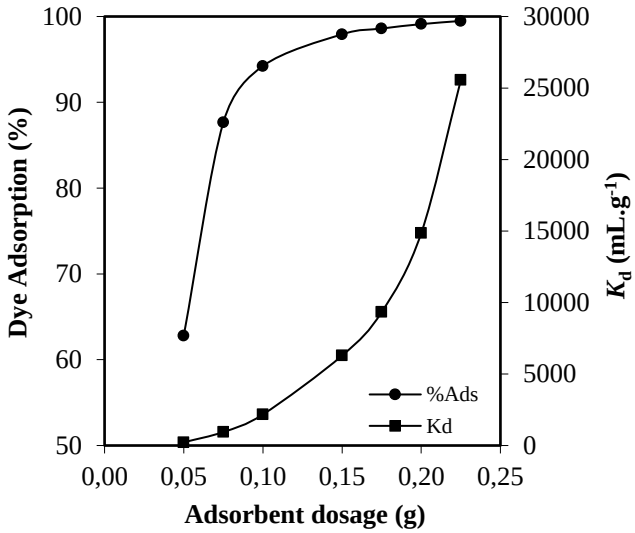

Figure 7: Effect of Adsorbent Dosage on the Efficiency of RN-RGB 150 Ion Adsorption onto PO-AC. (C_o = 463 mg.L^{-1}, Initial pH = 6.00, Contact time = 180 min., Particle size = 20>63 <74µm, Temperature = 303.15 K)

3.2.4. Effect of Temperature

In experiments conducted with a solution of RN-RGB 150 at a concentration of 463 mg.L^{-1}, 0.075 g of PO-AC was used. In addition, the experiments were conducted at an agitation speed of 125 rpm, with the experimental durations set to 180 minutes. Under these conditions, experiments were conducted between 288.15 and 318.15 K to examine the effect of temperature on the adsorption capacity of PO-AC, and the findings are presented in Figure 8.

Numerous studies have consistently demonstrated that elevated temperatures expedite the diffusion of adsorbate molecules. This phenomenon is primarily ascribed to the diminished solution viscosity and augmented molecular kinetic energy at higher temperatures. It has been extensively demonstrated that elevated temperatures lead to a significant increase in the removal rate. This phenomenon can be primarily ascribed to the intensified chemical interactions between adsorbates and adsorbents, coupled with the emergence of novel adsorption sites at higher temperatures (Tan et al., 2008).

It is widely acknowledged that temperature change has a significant impact on the adsorbent's equilibrium capacity for the adsorbate, and this augmented capacity translates into an accelerated removal rate with increasing temperature. It is well established that temperature variation has a significant impact on the physical bonds between the dye molecules and the active sites of the adsorbent, the solubility of the paints, and the interaction forces between the solute and the solvent. The weakening of physical bonds, increased solubility, and enhanced interaction forces collectively contribute to the observed phenomenon (Chen et al., 2010).

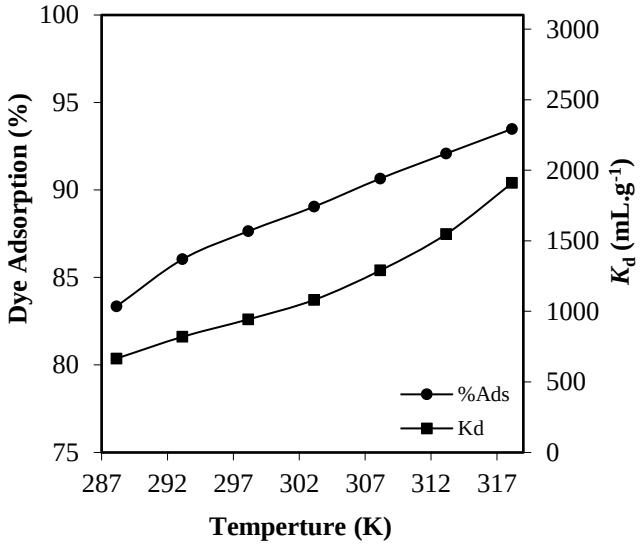

Figure 8: The Effect of Temperature on the Efficiency of RN-RGB 150 Ion Adsorption onto PO-AC (Adsorbent dosage = 0.075 g, C_o = 463 mg.L^{-1}, Initial pH = 6.00, Contact time = 180 min., Particle size = 20>63 <74µm)

The thermodynamic parameters obtained based on the graph are detailed in the table (Table 1.). Adsorption studies indicating an exothermic reaction with a negative enthalpy change suggest that the reaction releases more heat at higher temperatures, potentially due to a destabilization of the adsorbed species. In the present study, the entropy change

(ΔS) of the reaction was observed to be positive. This finding suggests that the entropy of the system increases and disorderliness increases as the reaction proceeds.

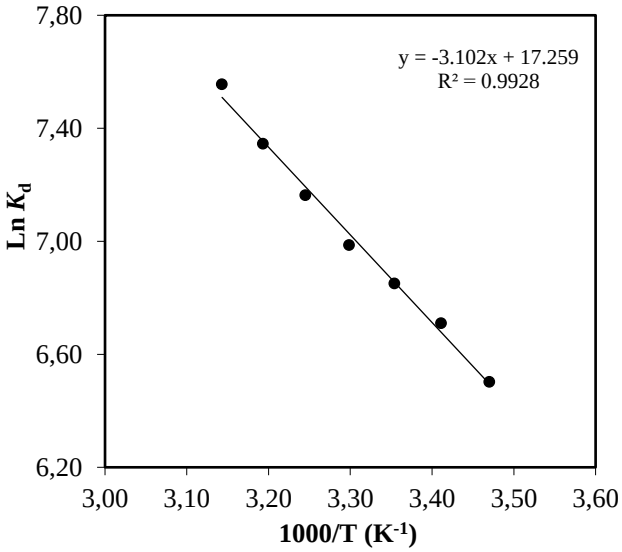

Figure 9: Langmuir Isotherm Plot for RN-RGB 150 Ion Adsorption onto PO-AC

Table 1: Thermodynamic Characterization of RN-RGB 150 Adsorption onto PO-AC.

ΔH° (kJ.mol^{-1})	ΔS° (kJ.mol^{-1}.K^{-1})	ΔG° (kJ.mol^{-1})						
25.79	0.14	288.15 K	293.15 K	298.15 K	303.15 K	308.15 K	313.15 K	318.15 K
		-15.56	-16.27	-17.00	-17.71	-18.43	-19.14	-19.86

3.2.5. Adsorption Isotherms

Various adsorption isotherms, such as Freundlich and Langmuir, allow us to better understand the mechanism and interactions of adsorption processes by examining the relationship between the adsorbent and adsorbate.

The remarkable fit of the experimental isotherm data to the Langmuir isotherm model is indicative of a homogeneous adsorption process characterized by monolayer formation. Furthermore, a comprehensive analysis of the experimental data reveals that chemical adsorption is the dominant mechanism responsible for the observed interactions between the adsorbate and the adsorbent surface.

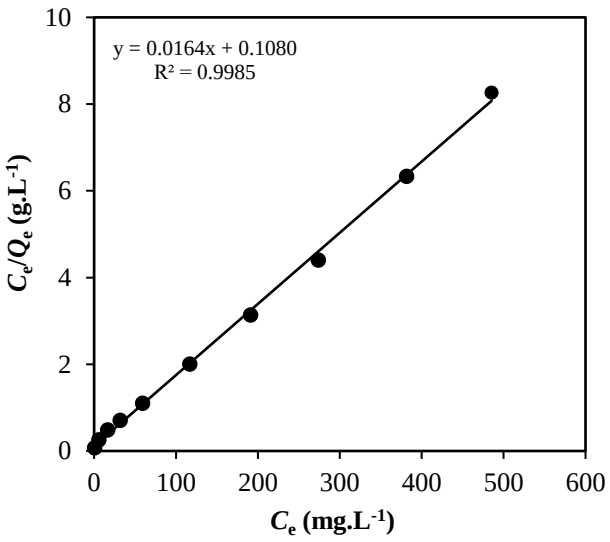

Figure 10: Langmuir Isotherm of RN-RGB 150 Ion Adsorption onto PO-AC

4. Discussion and Conclusion

The present study describes the development and characterization of an activated carbon adsorbent derived from *Posidonia Oceanica* seagrasses (PO-AC) using FTIR, SEM, and BET methods. 0.075 g adsorbent dosage and 3 h of contact time is sufficient to separate over 99% of RN-RGB 150 from the aqueous solution loaded with 463 $mg.L^{-1}$ RN-RGB 150 ions at 303.15 K.

To investigate the influence of temperature on adsorption, the thermodynamic parameters ΔH^o (enthalpy change), ΔS^o (entropy change), and ΔG^o (Gibbs free energy change) were calculated. The study revealed a positive correlation between temperature and adsorption percentage, while the $\Delta G°$ value decreased with increasing temperature. This suggests that the adsorption process becomes more spontaneous and efficient at higher temperatures. Thermodynamic parameters: ΔH^o, ΔS^o, and ΔG^o were calculated as 25.79 $Kj.mol^{-1}$, 0.14 $Kj.mol^{-1}.K^{-1}$, and -17.71 $Kj.mol^{-1}$, respectively. Analysis of the equilibrium data revealed a fit to the linear Langmuir isotherm model, suggesting a homogeneous adsorption process with monolayer coverage. The study determined the PO-AC adsorption capacity to be 60.97 $mg.g^{-1}$ for monolayer coverage and 0.1519 $L.mg^{-1}$ for monomolecular adsorption.

The research revealed that the produced seagrass-based activated carbon adsorbent showed high efficiency in removing PO-AC ions from aqueous environments as an environmentally friendly alternative.

5. Acknowledge

We would like to thank the Department of Chemistry, Faculty of Science, Pamukkale University, for their contributions to the completion of this research.

References

[1] Akyıl, S., Aslani, M. A., & Aytaş, Ş. Ö. (1998). Distribution of uranium on zeolite X and investigation of thermodynamic parameters for this system. Journal of Alloys and Compounds, 271, 769-773.

[2] Albadarin, A. B., & Mangwandi, C. (2015). Mechanisms of Alizarin Red S and Methylene blue biosorption onto olive stone by-product: Isotherm study in single and binary systems. Journal of environmental management,164, 86-93.

[3] Ali, N., Ali, F., Ullah, I., Ali, Z., Duclaux, L., Reinert, L., ... & Ahmad, I. (2020). Organically modified micron-sized vermiculite and silica for efficient removal of Alizarin Red S dye pollutant from aqueous solution. Environmental Technology & Innovation, 19, 101001.

[4] Al-Tohamy, R., Ali, S. S., Li, F., Okasha, K. M., Mahmoud, Y. A. G., Elsamahy, T., ... & Sun, J. (2022). A critical review on the treatment of dye-containing wastewater: Ecotoxicological and health concerns of textile dyes and possible remediation approaches for environmental safety. Ecotoxicology and Environmental Safety, 231, 113160.

[5] Arabi, S., & Sohrabi, M. R. (2014). Removal of methylene blue, a basic dye, from aqueous solutions using nano-zerovalent iron. Water science and technology, 70(1), 24-31.

[6] Aravind, P., Selvaraj, H., Ferro, S., Neelavannan, G. M., & Sundaram, M. (2018). A one-pot approach: oxychloride radicals enhanced electrochemical oxidation for the treatment of textile dye wastewater trailed by mixed salts recycling. Journal of cleaner production, 182, 246-258.

[7] Brião, G. V., Jahn, S. L., Foletto, E. L., & Dotto, G. L. (2018). Highly efficient and reusable mesoporous zeolite synthetized from a biopolymer for cationic dyes adsorption. Colloids and Surfaces A: Physicochemical and Engineering Aspects, 556, 43-50.

[8] Belessi, V., Romanos, G., Boukos, N., Lambropoulou, D., & Trapalis, C. (2009). Removal of Reactive Red 195 from aqueous solutions by adsorption on the surface of TiO_2 nanoparticles. Journal of hazardous materials, 170(2-3), 836-844.

[9] Bożęcka, A., Orlof-Naturalna, M., & Kopeć, M. (2021). Methods of dyes removal from aqueous environment. Journal of Ecological Engineering, 22(9).

[10] Bulgariu, L., Escudero, L. B., Bello, O. S., Iqbal, M., Nisar, J., Adegoke, K. A., ... & Anastopoulos, I. (2019). The utilization of leaf-based adsorbents for dyes removal: A review. Journal of Molecular Liquids, 276, 728-747.

[11] Chang, Y. M., Tsai, W. T., & Li, M. H. (2015). Chemical characterization of char derived from slow pyrolysis of microalgal residue. Journal of analytical and applied pyrolysis, 111, 88-93.

[12] Chen, S., Zhang, J., Zhang, C., Yue, Q., Li, Y., & Li, C. (2010). Equilibrium and kinetic studies of methyl orange and methyl violet adsorption on activated carbon derived from Phragmites australis. Desalination, 252(1-3), 149-156.

[13] Dawood, S., Sen, T. K., & Phan, C. (2018). Performance and dynamic modelling of biochar and kaolin packed bed adsorption column for aqueous phase methylene blue (MB) dye removal. Environmental technology.

[14] Ding, L., Zou, B., Gao, W., Liu, Q., Wang, Z., Guo, Y., ... & Liu, Y. (2014). Adsorption of Rhodamine-B from aqueous solution using treated rice husk-based activated carbon. Colloids and Surfaces A: Physicochemical and Engineering Aspects, 446, 1-7.

[15] Dutta, S., Gupta, B., Srivastava, S. K., & Gupta, A. K. (2021). Recent advances on the removal of dyes from wastewater using various adsorbents: A critical review. Materials Advances, 2(14), 4497-4531.

[16] Freundlich, H. (1907). Über die adsorption in lösungen. Zeitschrift für physikalische Chemie, 57(1), 385-470.

[17] Gokulan, R., Ganesh Prabhu, G., & Jegan, J. (2019). A novel sorbent Ulva lactuca-derived biochar for remediation of Remazol Brilliant Orange 3R in packed column. Water Environment Research, 91(7), 642-649.

[18] Goswami, M., & Phukan, P. (2017). Enhanced adsorption of cationic dyes using sulfonic acid modified activated carbon. Journal of Environmental Chemical Engineering, 5(4), 3508-3517.

[19] Gupta, N., Kushwaha, A. K., & Chattopadhyaya, M. C. (2012). Adsorptive removal of Pb^{2+}, Co^{2+} and Ni^{2+} by hydroxyapatite/chitosan composite from aqueous solution. Journal of the Taiwan Institute of Chemical Engineers, 43(1), 125-131.

[20] Hassan, N., Shahat, A., El-Didamony, A., El-Desouky, M. G., & El-Bindary, A. A. (2020). Mesoporous iron oxide nano spheres for capturing organic dyes from water sources. Journal of Molecular Structure, 1217, 128361.

[21] Hien, N. T., Nguyen, L. H., Van, H. T., Nguyen, T. D., Nguyen, T. H. V., Chu, T. H. H., ... & Aziz, K. H. H. (2020). Heterogeneous catalyst ozonation of Direct Black 22 from aqueous solution in the presence of metal slags originating from industrial solid wastes. Separation and Purification Technology, 233, 115961.

[22] Ho, Y. S. (2014). The real pseudo-second-order rate equation. Industrial Crops & Products, (52), 17.

[23] Homem, N. C., Beluci, N. D. C. L., Amorim, S., Reis, R., Vieira, A. M. S., Vieira, M. F., ... & Amorim, M. T. P. (2019). Surface modification of a polyethersulfone microfiltration membrane with graphene oxide for reactive dyes removal. Applied Surface Science, 486, 499-507.

[24] Kadhom, M., Albayati, N., Alalwan, H., & Al-Furaiji, M. (2020). Removal of dyes by agricultural waste. Sustainable Chemistry and Pharmacy, 16, 100259.

[25] Kang, Y. G., Yoon, H., Lee, C. S., Kim, E. J., & Chang, Y. S. (2019). Advanced oxidation and adsorptive bubble separation of dyes using MnO2-coated Fe3O4 nanocomposite. Water research, 151, 413-422.

[26] Khan, A. S., & Khan, A. M. (1995). Adsorption of chromium (III), Chromium (VI) and Silver (I) on bentonite. WASTE MANAGEMENT-PERGAMON PRESS-, 15, 271-282.

[27] Kumar, M., Gokulan, R., Sujatha, S., Shanmuga Priya, S. P., Praveen, S., & Elayaraja, S. (2021). Biodecolorization of Reactive Red 120 in batch and packed bed column using biochar derived from Ulva reticulata. Biomass Conversion and Biorefinery, 1-15.

[28] Langmuir, I. (1916). The constitution and fundamental properties of solids and liquids. Part I. Solids. Journal of the American chemical society, 38(11), 2221-2295.

[29] Li, Y., Zhang, X., Yang, R., Li, G., & Hu, C. (2016). Removal of dyes from aqueous solutions using activated carbon prepared from rice husk residue. Water Science and Technology, 73(5), 1122-1128.

[30] Liu, B., Zheng, H., Wang, Y., Chen, X., Zhao, C., An, Y., & Tang, X. (2018a). A novel carboxyl-rich chitosan-based polymer and its application for clay flocculation and cationic dye removal. Science of the total environment, 640, 107-115.

[31] Liu, L., Fan, S., & Li, Y. (2018b). Removal behavior of methylene blue from aqueous solution by tea waste: kinetics, isotherms and mechanism. International journal of environmental research and public health, 15(7), 1321.

[32] Madan, S., Shaw, R., Tiwari, S., & Tiwari, S. K. (2019). Adsorption dynamics of Congo red dye removal using ZnO functionalized high silica zeolitic particles. Applied Surface Science, 487, 907-917.

[33] Reda, M.M., & Sayeda, M.A. (2018). The efficacy of microalgal biomass collected from high rate algal pond for dyes biosorption and biofuel production. Res J Chem Environ, 22(11), 54-60.

[34] Nachiyar, C. V., Rakshi, A. D., Sandhya, S., Jebasta, N. B. D., & Nellore, J. (2023). Developments in treatment technologies of dye-containing effluent: A review. Case Studies in Chemical and Environmental Engineering, 100339.

[35] Nurhadi, M., Kusumawardani, R., Wirhanuddin, W., Gunawan, R., & Nur, H. (2019). Carbon-containing hydroxyapatite obtained from fish bone as low-cost mesoporous material for methylene blue adsorption. Bulletin of Chemical Reaction Engineering & Catalysis, 14(3), 660-671.

[36] Obaid, F. H., & Ali, L. A. M. (2023, February). Adsorption of the textile dye (reactive black 5) using orange peels as an adsorbent low-cost. In AIP Conference Proceedings (Vol. 2414, No. 1). AIP Publishing.

[37] Pandya, K. Y., Patel, R. V., Jasrai, R. T., & Brahmbhatt, N. H. (2017). Preliminary study on potential of seaweeds in decolorization efficacy of synthetic dyes effluent. Int. J. Plant Anim. Environ. Sci, 7, 223-4490.

[38] Pathania, D., Sharma, S., & Singh, P. (2017). Removal of methylene blue by adsorption onto activated carbon developed from Ficus carica bast. Arabian journal of chemistry, 10, S1445-S1451.

[39] Peng, Q., Yu, F., Huang, B., & Huang, Y. (2017). Carbon-containing bone hydroxyapatite obtained from tuna fish bone with high adsorption performance for Congo red. RSC advances, 7(43), 26968-26973.

[40] Pereira, L. A., Couto, A. B., Almeida, D. A. L., & Ferreira, N. G. (2020). Singular properties of boron-doped diamond/carbon fiber composite as anode in Brilliant Green dye electrochemical degradation. Diamond and Related Materials, 103, 107708.

[41] Rasheed, T., Bilal, M., Hassan, A. A., Nabeel, F., Bharagava, R. N., Ferreira, L. F. R., ... & Iqbal, H. M. (2020). Environmental threatening concern and efficient removal of pharmaceutically active compounds using metal-organic frameworks as adsorbents. Environmental research, 185, 109436.

[42] Saleem, M. M. R. J., Afzal, M., Qadeer, R., & Hanif, J. (1992). Selective adsorption of uranium on activated charcoal from electrolytic aqueous solutions. Separation Science and Technology, 27(2), 239-253.

[43] Samei, M., Sarrafzadeh, M. H., & Faramarzi, M. A. (2019). The impact of morphology and size of zinc oxide nanoparticles on its toxicity to the freshwater microalga, Raphidocelis subcapitata. Environmental Science and Pollution Research, 26, 2409-2420.

[44] Stella Mary, G., Sugumaran, P., Niveditha, S., Ramalakshmi, B., Ravichandran, P., & Seshadri, S. (2016). Production, characterization and evaluation of biochar from pod (Pisum sativum), leaf (Brassica oleracea) and peel (Citrus sinensis) wastes. International Journal of Recycling of Organic Waste in Agriculture, 5, 43-53.

[45] Tan, I. A. W., Ahmad, A. L., & Hameed, B. H. (2008). Enhancement of basic dye adsorption uptake from aqueous solutions using chemically modified oil palm shell activated carbon. Colloids and Surfaces A: Physicochemical and Engineering Aspects, 318(1-3), 88-96.

[46] Tural, B., Ertaş, E., Enez, B., Fincan, S. A., & Tural, S. (2017). Preparation and characterization of a novel magnetic biosorbent functionalized with biomass of Bacillus Subtilis: Kinetic and isotherm studies of biosorption processes in the removal of Methylene Blue. Journal of Environmental Chemical Engineering, 5(5), 4795-4802.

[47] Wanyonyi, W. C., Onyari, J. M., & Shiundu, P. M. (2013). Adsorption of methylene blue dye from aqueous solutions using Eichhornia crassipes. Bulletin of environmental contamination and toxicology, 91, 362-366.

[48] Wawrzkiewicz, M., Polska-Adach, E., & Hubicki, Z. (2019). Application of titania based adsorbent for removal of acid, reactive and direct dyes from textile effluents. Adsorption, 25, 621-630.

[49] Wu, J., Yang, J., Feng, P., Huang, G., Xu, C., & Lin, B. (2020). High-efficiency removal of dyes from wastewater by fully recycling litchi peel biochar. Chemosphere, 246, 125734.

[50] Yang, J., & Qiu, K. (2010). Preparation of activated carbons from walnut shells via vacuum chemical activation and their application for methylene blue removal. Chemical Engineering Journal, 165(1), 209-217.

[51] Zhang, L., Shao, Q., & Xu, C. (2019). Enhanced azo dye removal from wastewater by coupling sulfidated zero-valent iron with a chelator. Journal of cleaner production, 213, 753-761.

[52] Zhang, S., Dong, Q., Zhang, L., & Xiong, Y. (2015). High quality syngas production from microwave pyrolysis of rice husk with char-supported metallic catalysts. Bioresource technology, 191, 17-23.